that the position of the absorption maximum is dictated by the conformation of the In_6 chain, which describes approximately half a rotation of a screw-like helical progression (fig. S1).

Conformational effects have been widely commented upon in polysilane chemistry (*23*) and it appears likely that the chain conformation of compound **5** is constrained by the steric demands of the *N*-xylyl substituted β-diketiminate supporting ligands. A space-filling representation of compound **5** (fig. S2), illustrates the highly efficient protection of the individual In-In bonds provided by the closely arrayed aryl and methyl ligand susbstituents.

We have undertaken preliminary density functional theory (DFT) analysis (B3LYP/LANDZ) of the model linear In_6 complex $InIL(InL)_4InIL$ [where L is $(HNCH)_2CH$], **6**, constrained to the conformation described by the crystallographic coordinates from the x-ray analysis (*24*). These results provide a qualitative molecular orbital analysis of the bonding along a catenated hexa-indium chain (Fig. 3). The orbitals denoted lowest unoccupied molecular orbital (LUMO) to LUMO+4 are entirely ligand-based, whereas the LUMO+5 is the lowest energy unoccupied virtual orbital involved in In-In σ bonding. Unsurprisingly, the calculated LUMO+5 to highest occupied molecular orbital (HOMO) energy difference for the simplified complex **6** somewhat underestimates the σ-σ* transition energy (389 nm) inferred from the spectroscopic data provided by **5**. More exacting analysis will be required to fully appreciate the effects of differing substituent patterns as well as chain conformation.

References and Notes

1. J. E. Huheey, E. A. Keiter, R. L. Keiter, *Inorganic Chemistry* (Harper, New York, ed. 4, 1995).
2. For a recent review of group 13 cluster chemistry, see H. Schnöckel, *Dalton Trans.* **2005**, 3131 (2005).
3. D. G. Tuck, *Chem. Soc. Rev.* **22**, 270 (1993), and references therein.
4. D. G. Tuck, *Polyhedron* **9**, 377 (1990), and references therein.
5. For a recent comprehensive review of relevant literature, see W. Uhl, *Adv. Organomet. Chem.* **51**, 53 (2004).
6. A. Schnepf, C. Doriat, E. Mülhausen, H. Schnöckel, *Chem. Commun.* **1997**, 2111 (1997).
7. P. J. Brothers *et al.*, *Angew. Chem. Int. Ed. Engl.* **35**, 2355 (1996).
8. M. S. Hill, P. B. Hitchcock, *Chem. Commun.* **2004**, 1818 (2004).
9. M. S. Hill, P. B. Hitchcock, R. Pongtavornpinyo, *Angew. Chem. Int. Ed. Engl.* **44**, 4231 (2005).
10. P. J. Davidson, M. F. Lappert, *J. Chem. Soc. Chem. Commun.* **1973**, 317a (1973).
11. Although Et_2Sn was first reported in 1853 by Frankland, this material was undoubtedly polymeric. For a perspective on the early literature and structural work performed during the 1960s and 1970s, see (*25*).
12. S. Adams, M. Dräger, *Angew. Chem. Int. Ed. Engl.* **26**, 1255 (1987).
13. L. R. Sita, *Organometallics* **11**, 1442 (1992).
14. T. Imori, V. Lu, H. Cai, T. D. Tilley, *J. Am. Chem. Soc.* **117**, 9931 (1995).
15. N. Devylder, M. Hill, K. C. Molloy, G. J. Price, *Chem. Commun.* **1996**, 711 (1996).
16. K. Shibata, C. S. Weinert, L. R. Sita, *Organometallics* **17**, 2241 (1998).
17. M. Stender, P. P. Power, *Polyhedron* **21**, 525 (2002).
18. W. Uhl, M. Layh, W. Hiller, *J. Organomet. Chem.* **368**, 139 (1989).
19. N. Wiberg, K. Amelunxen, K. Nöth, H. Schmidt, H. Schwenk, *Angew. Chem. Int. Ed. Engl.* **35**, 65 (1996).
20. A. J. Downs, *Chemistry of Aluminium, Gallium, Indium, and Thallium* (Chapman, London, 1993).
21. M. Stender *et al.*, *Inorg. Chem.* **40**, 2794 (2001).
22. For a recent review, see I. Manners, *Synthetic Metal-Containing Polymers* (Wiley, Weinheim, 2004).
23. H. A. Fogarty *et al.*, *Pure Appl. Chem.* **75**, 999 (2003).
24. M. J. Frisch *et al.*, Gaussian 03, Revision C.02, Gaussian, Incorporated, Wallingford, CT (2004).
25. W. P. Neumann, in *The Organometallic and Coordination Chemistry of Germaninum, Tin, and Lead*, M. Gielen, P. G. Harrison, Eds. (Freund, Tel Aviv, 1978), p. 71.

26. We thank the Royal Society for funding this work via a University Research Fellowship for M.S.H. Full metrical parameters for the crystal structure of compound **5** are available free of charge from the Cambridge Crystallographic Data Center under reference CCDC 299581.

Supporting Online Material

www.sciencemag.org/cgi/content/full/311/5769/1904/DC1
Materials and Methods
SOM Text
Figs. S1 and S2
Table S1

16 December 2005; accepted 1 March 2006
10.1126/science.1123945

Rotational Coherence and a Sudden Breakdown in Linear Response Seen in Room-Temperature Liquids

Amy C. Moskun,[1]* Askat E. Jailaubekov,[1] Stephen E. Bradforth,[1]† Guohua Tao,[2] Richard M. Stratt[2]†

Highly energized molecules normally are rapidly equilibrated by a solvent; this finding is central to the conventional (linear-response) view of how chemical reactions occur in solution. However, when a reaction initiated by 33-femtosecond deep ultraviolet laser pulses is used to eject highly rotationally excited diatomic molecules into alcohols and water, rotational coherence persists for many rotational periods despite the solvent. Molecular dynamics simulations trace this slow development of molecular-scale friction to a clearly identifiable molecular event: an abrupt liquid-structure change triggered by the rapid rotation. This example shows that molecular relaxation can sometimes switch from linear to nonlinear response.

One of the principal ways in which a solvent facilitates a chemical reaction is by managing the energetics, both by supplying enough energy to surmount activation barriers and by providing channels for excess energy to be dissipated. Given the energies typically involved in chemical bond rearrangement (tens of kcal/mol, or roughly 10^4 K), these are formidable tasks for a solvent armed with no more than ordinary equilibrium (300 K) fluctuations. Nonetheless, as increasingly microscopic studies of solvation and vibrational relaxation have made clear, solvents do fulfill this critical energy management role, and they do so with precisely the rates expected from the solvent's own ability to absorb energy under ordinary equilibrium conditions (*1*).

This idea that excited states relax with rates determined by the solute-solvent system's ordinary energy fluctuations, commonly called linear response theory, is a critical component in the success of transition-state theories of chemical reaction rates in liquids (*2*). Perhaps a surprising consequence of linear response theory is that the details of how a solute's state is prepared—in particular, how much energy is deposited—are not central to determining how quickly a solvent responds. Even though linear response theory is often derived by assuming relatively small displacements from equilibrium (*3*)—an assumption clearly inappropriate for the amounts of energy relevant to most chemical reactions—it seems to hold rather well, a few notable exceptions aside (*4*–*7*). However, three decades of work in the gas phase have explored how the specifics of the forces between atoms involved in isolated chemical reactions determine the final energy partitioning as the reaction moves from the transition state (*8*). Is knowledge of these specifics completely immaterial (*2*) to reaction dynamics in solution?

This dichotomy highlights a principal difference between gas- and solution-phase chemical dynamics: In low-density gases, the natural perspective focuses on discrete collisions between individual molecules, whereas in the condensed phase, a solute's environment is typically treated collectively and its dynamics are

[1]Department of Chemistry, University of Southern California, Los Angeles, CA 90089, USA. [2]Department of Chemistry, Brown University, Providence, RI 02912, USA.

*Present address: Department of Chemistry, University of California, Irvine, CA 92697, USA.

†To whom correspondence should be addressed. E-mail: bradfort@usc.edu (S.E.B.); richard_stratt@brown.edu (R.M.S.)

described in terms of the evolution of chance fluctuations from equilibrium (*1*). Consider the rotational motion of a solute molecule in a liquid. From the collisional viewpoint, the onset of rotational diffusion can be construed in terms of Brownian small-angle reorientation (*9*), where collisions rapidly interrupt and destroy the coherence of an isolated rotor ensemble. This picture implies that there must be some limited time interval over which inertial (gas phase–like) rotation survives, but at normal liquid densities and temperatures this interval usually corresponds to the solute sweeping out no more than a very small angle. This inertial behavior has been observed for solute reorientation in liquids in only a few, rather weakly interacting, cases (*10*–*12*). The usual condensed-phase perspective, by contrast, is that there are no specific events through which the liquid begins to exert its influence; linear response theory dictates that random solvent fluctuations simply extract more and more of the rotor's energy as time goes on.

Consider, then, what happens if a solute is born with extremely high rotational energy. Gas-phase intuition suggests that there may be a much longer period, perhaps more than an entire rotational period, during which entirely gas phase–like dynamics might prevail and the solvent would be unable to disrupt the solute. If so, what does this say about the solvent response in terms of linear response theory? We explore this issue by watching an example of rotational relaxation in a standard chemical environment: liquid water and alcohol solutions. By using a chemical reaction to prepare a high-energy, nonthermal ensemble of rotating diatomic molecules and following the subsequent relaxation on a subpicosecond time scale, we show that neither gas-phase nor liquid-phase intuition is entirely correct. The initial relaxation turns out to proceed just as linear response theory would predict, but the system abruptly reverts to much more gas phase–like dynamics. Such a switch can apparently be attributed directly to specific molecular events occurring in the liquid.

We use ICN photodissociation (*13*, *14*), a chemical reaction in which bond breakage is nearly instantaneous in the gas phase (*15*), leading to a well-characterized, coherent population of highly excited CN rotors with virtually none of the excess energy channeled into CN vibration (*16*, *17*). Although the reaction also has a channel producing cold CN fragments (roughly 60% of the time in the gas phase), the average energy of the hot rotors can be tuned by varying the photoexcitation wavelength, enabling us to generate a controlled and predetermined high-energy distribution of initial rotational states (*18*). In earlier work, Moskun and Bradforth (*19*) were able to show that this reaction also produces rotationally hot CN in room-temperature polar liquids. These results were themselves surprising. The hot rotors apparently act as if they were nearly freely spinning tops, maintaining their rotation plane for tens of rotational periods (several picoseconds). Seeing such gas phase–like behavior in an ordinary room-temperature molecular liquid runs counter to the conventional Brownian small-angle rotational diffusion picture of rotational relaxation, which would have suggested complete randomization of the axis of rotation in well under 1 ps (*9*). Multiple periods of free rotation would also be a striking change from earlier photodissociation studies on I_3^- and HgI_2 in solution, which saw only small-angle ballistic rotation (*20*, *21*).

These early CN solution experiments, though, were unable to capture the crucial first 200 fs of the dynamics because of insufficient time resolution as well as a strong coherent solvent response near time zero, a response broadened by the thickness of the interrogated liquid film. However, recent advances in ultrashort ultraviolet (UV) pulse generation have allowed us to perform a deep UV-pump/UV-probe experiment with the necessary time resolution. We create photolysis pulses with a wavelength of 233 nm (duration ~33 fs) by four-wave mixing in a rare gas–filled hollow-core fiber, followed by compression using a CaF_2 prism pair (*22*, *23*). Time-delayed 390-nm probe pulses, which monitor the CN product by transient absorption, are selected from a white-light continuum generated in a CaF_2 disk and compressed using a fused-silica prism pair (*18*). We interrogate the ICN solutions in alcohols and water by overlapping linearly polarized pump and probe pulses in a region of a flowing liquid film ~25 μm thick (*24*). The probe beam, polarized 45° relative to the pump, is resolved after the sample into parallel (∥) and perpendicular (⊥) components that are detected simultaneously with two photodiodes (*21*). The rotational relaxation is then tracked by watching the time-dependent anisotropy

$$R(t) = (A_{\parallel} - A_{\perp})/(A_{\parallel} + 2A_{\perp}) \qquad (1)$$

constructed from the two components of the transient probe absorbance $A(t)$.

Although anisotropy does not measure rotational energy relaxation directly, the tendency of rapidly rotating objects to maintain their rotational plane means that the loss of the initial anisotropy is a useful indicator of the loss of rotational energy. The anisotropy function is a vector correlation function and carries additional information about the ensemble motion, including its degree of rotational coherence. In an isotropic environment such as a fluid, the anisotropy is given by

$$R(t) = {}^2/_5\langle P_2[\hat{\Omega}(0) \cdot \hat{\Omega}(t)]\rangle \qquad (2)$$

which measures the angle between the time-0 and time-t transition-dipole vectors $\hat{\Omega}$ averaged over the initial distribution of rotor orientations and angular velocities (P_2 is the standard second-order Legendre polynomial). This same observable has long been used to extract rotational diffusion constants (*9*). However, on an ultrafast time scale, it can be far more informative about the underlying microscopic behavior (Fig. 1).

The anisotropy of free CN rotors prepared with a rotational energy E_{ROT} of precisely 1998 cm^{-1} at time 0 [equivalent to 2875 K of rotational energy and corresponding to rotational quantum number $J \approx 32$, a typical value for ICN photodissociation (*16*)] is compared in Fig.

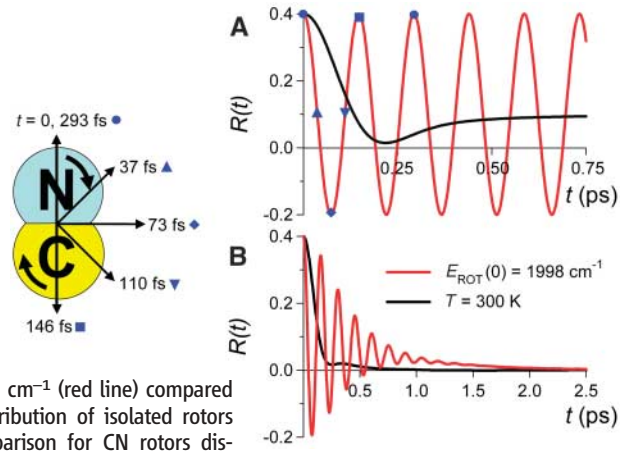

Fig. 1. The connection between transient anisotropy $R(t)$ and the dynamics of molecular reorientation predicted by a classical molecular dynamics simulation. In the experiment reported here, $R(t)$ measures the correlation between the CN bond axis at the instant of photodissociation and the same axis of the CN fragment after elapsed time t. (**A**) Anisotropy evolution of an isolated rotor prepared with a precise rotational energy of 1998 cm^{-1} (red line) compared to that of a 300 K thermal distribution of isolated rotors (black line). (**B**) The same comparison for CN rotors dissolved in 300 K liquid-density (1.344 g/ml) Ar. It is clear from the symbols corresponding to rotations of 0°, 45°, 90°, 135°, 180°, and 360° (as shown at left) that the anisotropy of the single-energy isolated rotor tracks the molecular orientation perfectly, displaying exactly two oscillations for every 360° molecular rotation. Thermal preparation of the rotor evidently destroys too much phase information to carry out such tracking (whether a solvent is present or not), but high-energy rotors can be tracked even in the presence of a solvent; enough of the rotational coherence survives the solvent-induced dephasing for several full rotations to be observable.

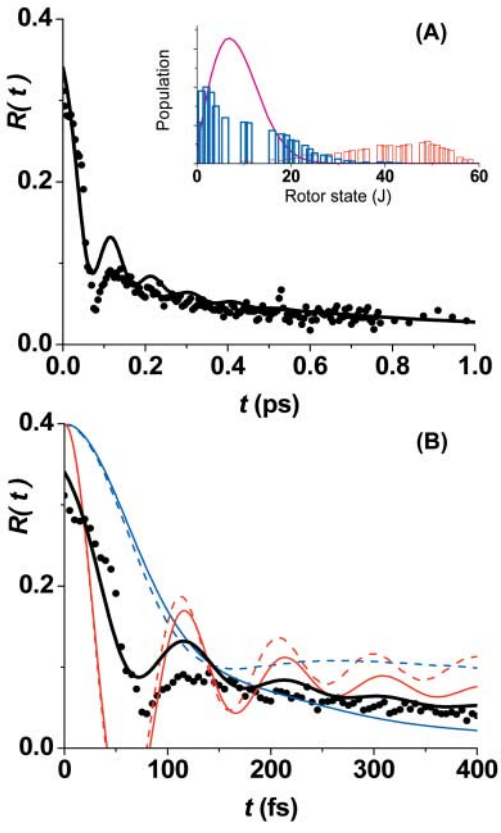

Fig. 2. (**A**) Measured transient pump-probe anisotropy after 233-nm photodissociation of ICN in ethanol (circles). The inset shows the highly non-Boltzmann initial populations of CN fragments in the rotationally hot (red) and cold (blue) channels resulting from this photodissociation in the gas phase (*16*); for comparison, a 300 K thermal rotational distribution is also shown (magenta curve). The gas-phase behavior of the two channels is assumed to carry over to the initial rotor distributions in the condensed phase. (**B**) Molecular dynamics predictions (on an expanded scale) for how each individual channel would contribute in a 300 K, 1.344 g/ml Ar solvent [solid curves; colors as in inset of (A)], contrasted with the behavior of free CN rotors (dashed curves) prepared with the same rotational energy distributions. The black solid curve in both panels is a prediction of the net anisotropy decay this experiment would have produced with a 300 K, liquid-density Ar solvent [calculated as a weighted sum of the solid colored curves corrected for the finite CN lifetime, and convoluted with the experimental response function (*18*)].

1A to the anisotropy for a 300 K equilibrium ensemble. A hypothetical experiment conducted using the perfect rotational coherence of the former (single-energy) ensemble would be able to associate individual points on the $R(t)$ curve with specific angle displacements of the CN radicals. With a thermal (300 K) distribution of rotational energies, by contrast, the anisotropy function would lose most of these oscillations because of the corresponding spread in angular frequencies, although for free rotors there would always be a minimum and the function would tend toward an asymptotic value of 0.1. Given these observations, one might imagine that carrying out the study in a 300 K liquid would remove most of this remaining detail, but as the classical molecular dynamics simulation in liquid-density Ar reveals (Fig.1B), rotational coherence can still be preserved for several rotational periods if the initial rotational energy distribution is sufficiently out of equilibrium with the liquid (*25*).

The simulations reported here were microcanonical, periodic boundary-condition studies conducted by sampling the classical trajectories of a single rigid CN diatomic instantaneously provided with a prescribed rotational kinetic energy in the presence of 106 Ar solvent atoms (*18*). We chose Ar not only for the simplifications it afforded in our subsequent analysis, but because it allowed us to use a high-level ab initio potential surface (*26*) capable of reproducing detailed gas-phase inelastic scattering measurements (*27*). But does this same coherent behavior persist with a more strongly interacting liquid? Our experimental results for 233-nm ICN photodissociation in liquid ethanol (Fig. 2) show that it can. The anisotropy of the CN rotors displays a local minimum at ~80 fs, quickly rises to ~0.1, and then decays over several picoseconds, exhibiting what seem to be weaker oscillations along the way (*28*). Similar results are seen in H_2O and D_2O and in methanol (fig. S5).

The experimental $R(t)$ curves would be expected to differ in a number of ways from the highly idealized oscillatory curve shown in Fig. 1B, but most of these effects are straightforward to characterize. The experiment's finite time resolution is simple to include. More fundamentally, both the hot and cold photodissociation channels produce relatively broad initial distributions of rotational (J) states, but the relevant gas-phase distributions for each channel are known from previous experimental measurement (*16*, *29*) (Fig. 2A, inset). The only important unknown is the liquid-state branching ratio between the two channels. Gas-phase data indicate that the hot channel makes up ~40% of the dissociation yield (*16*), but one might expect a somewhat higher figure for liquid solvents in view of the potential of the liquid to cage the cold photodissociation products (*13*).

Taking these factors into account, we can confirm that the persistent rotational coherence seen in our Ar simulations is the same basic phenomenon observed experimentally in polar solvents. Although CN rotors sampled from the cold-channel distribution undergo a rapid loss of anisotropy in liquid Ar (Fig. 2B, solid blue line), the rotors sampled from the hot-channel distribution retain almost as much coherence in the liquid (solid red line) as they would in the absence of solvent (dashed red line), despite the breadth of these initial distributions. Convolution of the simulation with the 45-fs experimental instrument response function, along with the assumption that liquid-state photodissociation generates an initial ensemble composed of a 60%/40% admixture of the hot and cold gas-phase distributions, yields the anisotropy decay curve (heavy black line) of a hypothetical repetition of this experiment in liquid Ar. The resulting oscillations are somewhat more pronounced in the more weakly interacting solvent than they are in ethanol, but the qualitative features and time scales of the experimental and theoretical curves are otherwise remarkably similar. [Assuming a more gas phase–like 40%/60% branching ratio would lower the amplitude of the predicted oscillations but would not affect their existence or time scales (*18*).]

This level of agreement gives us confidence that our idealized Ar simulations can be used to infer more detailed microscopic information about the development (or more correctly, the lack of development) of rotational friction about a rapidly rotating CN molecule. In simulations, for example, we can directly calculate the energy relaxation function for the actual trajectories

$$S_E(t) = [\overline{E}(t) - \overline{E}(\infty)]/[\overline{E}(0) - \overline{E}(\infty)] \quad (3)$$

where E refers to the rotational kinetic energy and the overbars imply an average over all the initial conditions consistent with the rotor's nonequilibrium preparation. We can then compare the results to the linear-response prediction

$$C_E(t) = [\langle E(0)E(t)\rangle - \langle E\rangle^2]/[\langle E^2\rangle - \langle E\rangle^2] \quad (4)$$

(*1*, *3*), where the angle brackets denote an average over the distribution of molecular velocities and positions that one would find under equilibrium (thermal) conditions.

The results (Fig. 3) show that linear response theory does indeed fail rather dramatically here (*30*): The actual relaxation is considerably slower than the equilibrium rotational energy fluctuations would have predicted, which explains the unexpected level of preservation of rotational coherence. But what is interesting is how this failure occurs. A close inspection of the first 200 fs for a range of different initial rotational energies (Fig. 3, lower panel) reveals that linear response is quantitatively correct for the first 50 to 100 fs—values suspiciously close

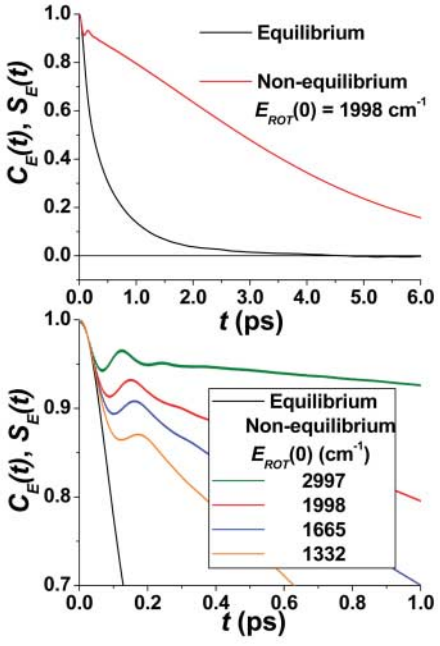

Fig. 3. Molecular dynamics simulation of the breakdown in linear response for hot CN rotors in liquid Ar at 120 K (density 1.344 g/ml). Both panels compare the rotational kinetic energy relaxation functions observed in the actual nonequilibrium simulations $S_E(t)$ (colored lines) with the corresponding linear-response prediction $C_E(t)$ (black line). The nonequilibrium simulations follow the rotational kinetic energy after a CN rotor is given a specific value $E_{ROT}(0)$ at time 0. By contrast, the linear-response curve looks only at the decay of ordinary equilibrium rotational energy fluctuations at the temperature of the liquid (even when extraordinary energies are to be dissipated). (**Top**) The linear-response answer compared with that from a single nonequilibrium calculation over a fairly long time period. (**Bottom**) The subpicosecond dynamics for four successively larger values of $E_{ROT}(0)$. In this panel, it is clear how linear response breaks down only after a well-defined time delay, which becomes increasingly protracted as the initial rotational energy decreases. At these energies, a 90° rotation of an isolated CN rotor would take 60, 73, 80, and 90 fs, respectively.

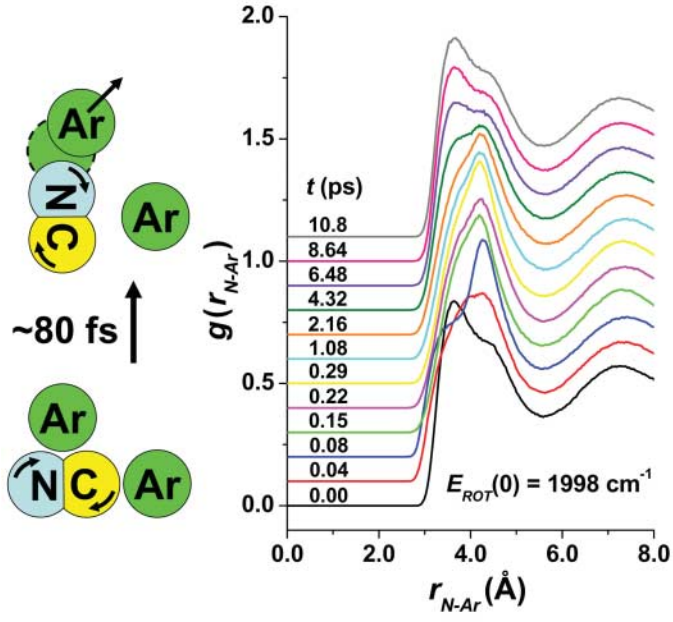

Fig. 4. Liquid-structure changes corresponding to a linear-response breakdown. Shown are molecular dynamics results for the relaxation of a single 1998 cm^{-1} CN rotor dissolved in liquid Ar (under the same conditions reported in Fig. 3). The plot reports the normalized probability densities of N-Ar distances $r_{N\text{-}Ar}$ in the CN-rotor plane (*18*) at the indicated times t after the rotational preparation. Successive curves are translated vertically for ease in viewing. The time-0 curve, in particular, shows the equilibrium structure, an arrangement that is not recovered until 9 to 10 ps later. The principal structural change occurs within 80 fs, the interval (as shown at left) that corresponds to the time needed for a CN to rotate ~90°, forcing a neighboring Ar atom out of the inner solvation shell.

to the 60 to 90 fs that it would take free rotors with these energies to rotate ~90°. Once this amount of molecular reorientation has occurred, though, the solvent evidently begins to function differently and the linear-response predictions begin to fail.

Given the existence of such a well-defined event, it is a simple matter to interrogate our simulations to discover just what the liquid is doing at the critical moment. We plot in Fig. 4 the radial distribution functions for the solvent atoms in the CN rotor plane. By looking at a function of the time elapsed after the rotational excitation, one can see that the liquid structure around the CN solute itself undergoes a relatively sudden change at roughly 80 fs: The loss of the peak at 3.8 Å and the corresponding growth of a peak at 4.5 Å means that a 90° rotation of a CN suffices to push at least some solvent atoms out of the innermost solvent shell. This expulsion of such nearby solvent atoms is what is probably responsible for the sudden diminishment of the local rotational friction. The fact that it then takes on the order of 10 ps for the liquid structure to recover from this first 0.1 ps is surprising, but is nicely consistent with the slow progress of the overall rotational relaxation (*19*).

The presence of a connection between nonlinear response and the evolution of liquid structure has been noted in a number of computer simulation studies of how linear response can fail during solvation (*4*–*6*), although there has never been any direct experimental evidence for such a scenario. In a typical simulation of solvation, the relaxation of the solute-solvent potential energy is monitored after an instantaneous change in the charge distribution of a solute, and linear response theory is found to yield accurate predictions even when solvation energies are greater than 10^4 K (*1*). But in a few cases involving hydrogen-bonding liquids (*4*–*6*) and solute size changes (*5*, *6*), the simulated solvation is noticeably different from predictions based on the solvent's normal equilibrium fluctuations. In each of these instances, it was clear that liquid-structure transformations must have been involved in some way because the liquid's local geometry was different before and after the solvation process. However, in this work, we have observed a discrete molecular event in the solvent, occurring at a specific time, that mediates the failure of linear response.

Our principal experimental result is the time-domain observation of largely free molecular rotation occurring in a strongly interacting room-temperature liquid. The preservation of such free rotation yields valuable clues about the course of energy dissipation in chemical processes. In particular, the observation of coherence tied to the original rotor time scale is direct evidence of a nonlinearly responding solvent. The experiment therefore provides a window into the ultrafast time evolution of not only the solute relaxation but the solvent structure. Moreover, the possibility of controlling the specifics of the preparation of our rotors offers us yet other opportunities, including the chance to learn about some of the key issues germane to solution photochemistry: how a solvent affects the dynamics of an electronic curve crossing and whether cage recombination (*13*, *14*) selects out particular subpopulations of solute states.

References and Notes

1. R. M. Stratt, M. Maroncelli, *J. Phys. Chem.* **100**, 12981 (1996).
2. G. A. Voth, R. M. Hochstrasser, *J. Phys. Chem.* **100**, 13034 (1996).
3. D. Chandler, *Introduction to Modern Statistical Mechanics* (Oxford Univ. Press, New York, 1987), chap. 8.
4. T. Fonseca, B. M. Ladanyi, *J. Phys. Chem.* **95**, 2116 (1991).
5. C. J. Smallwood, W. B. Bosma, R. E. Larsen, B. J. Schwartz, *J. Chem. Phys.* **119**, 11263 (2003).
6. L. Turi, P. Minary, P. J. Rossky, *Chem. Phys. Lett.* **316**, 465 (2000).
7. P. L. Geissler, D. Chandler, *J. Chem. Phys.* **113**, 9759 (2000).
8. R. Schinke, *Photodissociation Dynamics Spectroscopy and Fragmentation of Small Polyatomic Molecules* (Cambridge Univ. Press, Cambridge, 1993).
9. G. R. Fleming, *Chemical Applications of Ultrafast Spectroscopy* (Oxford Univ. Press, New York, 1986), sec. 6.2.

10. S. Grebenev, J. P. Toennies, A. F. Vilesov, *Science* **279**, 2083 (1998).
11. D. G. Taylor, H. L. Strauss, *J. Chem. Phys.* **90**, 768 (1989).
12. Y. Danten, T. Tassaing, M. Besnard, *J. Phys. Chem. A* **104**, 9415 (2000).
13. N. Winter, I. Chorny, J. Vieceli, I. Benjamin, *J. Chem. Phys.* **119**, 2127 (2003).
14. J. Larsen *et al.*, *J. Chem. Phys.* **116**, 7997 (2002).
15. M. Dantus, M. J. Rosker, A. H. Zewail, *J. Chem. Phys.* **89**, 6128 (1988).
16. I. Nadler, D. Mahgerefteh, H. Reisler, C. Wittig, *J. Chem. Phys.* **82**, 3885 (1985).
17. W. P. Marinelli, N. Sivakumar, P. L. Houston, *J. Phys. Chem.* **88**, 6685 (1984).
18. See supporting material on *Science* Online.
19. A. C. Moskun, S. E. Bradforth, *J. Chem. Phys.* **119**, 4500 (2003).
20. H. Bursing, P. Vohringer, *Phys. Chem. Chem. Phys.* **2**, 73 (2000).
21. T. Kuhne, P. Vohringer, *J. Phys. Chem. A* **102**, 4177 (1998).
22. A. E. Jailaubekov, S. E. Bradforth, *Appl. Phys. Lett.* **87**, 021107 (2005).
23. C. G. Durfee III, S. Backus, M. M. Murnane, H. C. Kapteyn, *Opt. Lett.* **22**, 1565 (1997).
24. M. J. Tauber, R. A. Mathies, X. Chen, S. E. Bradforth, *Rev. Sci. Instrum.* **74**, 4958 (2003).
25. Quantum mechanical features of the rotational dynamics are probably not a major concern in the analysis of our experiments: For CN rotors produced in the rotationally hot channel, the average initial rotational kinetic energy is on the order of 4700 K (15 times the 300 K thermal energy of the solvent), whereas the spacing of rotational energy levels corresponds to only 230 K. We therefore use the phrase "rotational coherence" to refer only to classical coherence, not to coherence in the quantum mechanical phase.
26. M. H. Alexander, X. Yang, P. J. Dagdigian, A. Berning, H. J. Werner, *J. Chem. Phys.* **112**, 781 (2000).
27. X. Yang, P. J. Dagdigian, M. H. Alexander, *J. Chem. Phys.* **112**, 4474 (2000).
28. The oscillatory behavior of the early signal is characteristic of coherent free rotation of hot CN, validating the assumption that the dissociation reaction is impulsive with respect to solvent motions.
29. Because of solvent shifts, the data reported for gas-phase photodissociation at 266 nm correspond to our liquid-state photolysis at 233 nm. See (*13*, *19*).
30. Although very similar nonlinear-response behavior is seen in our 300 K liquid-density supercritical Ar simulations, we report in Figs. 3 and 4 the results for the normal 120 K liquid.
31. We thank P. Pieniazek, A. Krylov, I. Benajmin, and M. Alexander for helpful discussions. Work at USC is supported by NSF grant CHE-0311814 and by the David and Lucile Packard Foundation, and at Brown by NSF grants CHE-0131114, CHE-0212823, and CHE-0518169.

Supporting Online Material

www.sciencemag.org/cgi/content/full/311/5769/1907/DC1
Materials and Methods
Figs. S1 to S7
References

12 December 2005; accepted 21 February 2006
10.1126/science.1123738

High-Performance High-T_c Superconducting Wires

S. Kang,[1] A. Goyal,[1]* J. Li,[1] A. A. Gapud,[1]† P. M. Martin,[1] L. Heatherly,[1] J. R. Thompson,[1,2] D. K. Christen,[1] F. A. List,[1] M. Paranthaman,[1] D. F. Lee[1]

We demonstrated short segments of a superconducting wire that meets or exceeds performance requirements for many large-scale applications of high-temperature superconducting materials, especially those requiring a high supercurrent and/or a high engineering critical current density in applied magnetic fields. The performance requirements for these varied applications were met in 3-micrometer-thick $YBa_2Cu_3O_{7-\delta}$ films epitaxially grown via pulsed laser ablation on rolling assisted biaxially textured substrates. Enhancements of the critical current in self-field as well as excellent retention of this current in high applied magnetic fields were achieved in the thick films via incorporation of a periodic array of extended columnar defects, composed of self-aligned nanodots of nonsuperconducting material extending through the entire thickness of the film. These columnar defects are highly effective in pinning the superconducting vortices or flux lines, thereby resulting in the substantially enhanced performance of this wire.

Second-generation high-temperature superconducting (HTS) wires or coated conductors (also known as 2G wires) based on $REBa_2Cu_3O_{7-\delta}$ (RE, rare earth) films have important potential for use in large-scale civilian and military applications (*1*–*3*). For many of these potential applications, large critical currents in high applied magnetic fields are required. This is especially so for electric power applications of HTS materials as well as for military applications. For example, the underground transmission cable application requires critical current per unit width, I_c, greater than 300 A/cm in self-field; for military applications, an I_c greater than 100 A/cm and an engineering critical current density, J_E, greater than 15 kA/cm^2 at 65 K in an operating field of 3 T are required; and for rotating machinery such as motors and generators, a J_E of 30 to 40 kA/cm^2 at 55 to 65 K in operating fields of 3 to 5 T is required.

Coated conductors consist of a flexible substrate (a metallic template with several buffer layers) and an epitaxial superconducting layer (*1*). The goal is to have a biaxially textured superconducting layer so that few if any high-angle, weakly conducting grain boundaries are present. Three techniques for producing biaxial texture in the substrate have been developed: ion beam–assisted deposition (IBAD) of biaxialy textured buffers on polycrystalline alloy substrates (*1*, *4*), epitaxial deposition of buffer multilayers on rolling assisted biaxially textured substrates (RABiTS) (*1*, *5*), and inclined substrate deposition of buffers on polycrystalline alloy substrates (*1*, *6*). For epitaxial HTS films on such textured substrates, the intergranular critical current density is substantially improved because of the elimination of weakly linked, high-angle grain boundaries. However, for practical application of HTS materials, the in-field performance, or the intragranular critical current density, also needs to be enhanced further. It is also essential to increase the overall current-carrying capacity of the coated conductors. The simplest approach is to increase the thickness of the superconductor. However, gradual deterioration of the critical current density occurs with increasing superconductor thickness. For films deposited by in situ techniques such as pulsed laser deposition (PLD), as the superconducting layer becomes thicker, a dead layer that provides no contribution to the current carrying ability forms after a critical thickness of ~1.5 μm (*7*). This has been attributed to roughening of the film with increase in thickness. A solution to this roughness problem was found by fabricating multilayered films with $YBa_2Cu_3O_{7-\delta}$ (YBCO) layers less than 1.5 μm thick alternating with intervening CeO_2 interlayers (*7*). Although there was no dead layer formation in these multilayer films, a single layer is still desirable because of the processing complexity in multilayer growth. We have overcome this problem by manipulation of deposition conditions and substrate characteristics and have demonstrated growth of a 6.4-μm-thick single-layer YBCO film on RABiTS without the formation of any dead layer (*8*, *9*). However, for both the multilayered films and the single-layer-thick films without a dead layer, further improvement in the in-field transport properties is needed to meet the performance requirements for a range of applications. This can be accomplished by improving the flux pinning by introducing appropriate defects into the films.

It is known that defects within superconducting materials can pin the magnetic flux lines, so that large currents can flow through the materials in the presence of high applied magnetic fields. However, in order for the defects to be effective in pinning the flux, their size, density, and geometry need to be appropriately controlled. Defects such as oxygen vacancies, twin boundaries (*10*), and dislocations (*11*, *12*) form naturally inside films and act as pinning centers.

[1]Oak Ridge National Laboratory, Oak Ridge, TN 37831, USA. [2]Department of Physics, University of Tennessee, Knoxville, TN 37996, USA.

*To whom correspondence should be addressed. E-mail: goyala@ornl.gov
†Present address: Department of Physics, University of South Alabama, ILB 103, Mobile, AL 36688, USA.